Research Article | Vol. 28, No. 7 / 30 March 2020 / Optics Express 10400
Optics EXPRESS

Crosstalk reduction for multi-channel optical phase metrology

PAUL G. SIBLEY,[1,2,3,4,*] ROBERT L. WARD,[1,2] LYLE E. ROBERTS,[1,2] SAMUEL P. FRANCIS,[1,2] AND DANIEL A. SHADDOCK[1,2,3]

[1] *Centre for Gravitational Astrophysics, College of Science, Australian National University, Australia*
[2] *OzGrav-ANU, Research School of Physics, Australian National University, Australia*
[3] *ARC Centre for Engineered Quantum Systems, Research School of Physics, Australian National University, Australia*
[4] *Space Environment Research Centre (SERC), Advanced Instrumentation and Technology Centre, Mt. Stromlo Observatory, Australia*
[*] *paul.sibley@anu.edu.au*

Abstract: Digitally enhanced heterodyne interferometry (DEHI) combines the sub-wavelength displacement measurements of conventional laser interferometry with the multiplexing capabilities of spread-spectrum modulation techniques to discriminate between multiple electric fields at a single photodetector. Technologies that benefit from DEHI include optical phased arrays, which require the simultaneous phase measurement of a large number of electric fields. A consequence of measuring the phase of multiple electric fields is the introduction of crosstalk, which can degrade measurement precision. This work analytically and experimentally investigates the crosstalk when using DEHI to measure the phase of an arbitrarily large number of electric fields at a single photodetector. Also considered is the practical limit the dynamic range of the photodetector and shot noise imposes on the number of electric fields that can be discriminated. We describe how to minimize crosstalk by design. Experimental results demonstrate up to 55 dB suppression of crosstalk between two electric fields with a phase measurement bandwidth of 20 kHz and 1-10 pm/$\sqrt{\text{Hz}}$ displacement sensitivity for audio frequencies. Additionally, we demonstrate scaling of crosstalk proportional to the square-root of the number of electric fields when using an M-sequence modulation. Based on this analysis, we estimate that digitally enhanced heterodyne interferometry should be capable of measuring the phase of several hundreds of electric fields at a single photodetector while maintaining the same measurement bandwidth.

1. Introduction

Digitally enhanced interferometry enables the discrimination of multiple interferometric signals at a single photodetector without sacrificing the sub-wavelength sensitivity of conventional laser interferometry [1]. The technique works by encoding an optical carrier with a known pseudo-random binary sequence (PRBS), allowing isolation of signals based on the correlation properties of the PRBS. Similar spread-spectrum techniques have been applied for some time in radio communications [2] and more recently in optical communications [3] (OCDMA) as well as for ranging (e.g. in GPS). In Digitally Enhanced Heterodyne Interferometry (DEHI), the use of pseudo-random sequences is combined with heterodyne interferometry to achieve simultaneous high precision measurements of optical phase.

Combining signal multiplexing techniques and precision displacement metrology through interferometry has enabled the development of a range of multi-point sensors. In particular, this has benefitted optical phased arrays (OPA), which lock the phase of multiple optical fields for controlled coherent beam combination. Techniques to enable the multiplexing of optical phase measurements developed for OPAs include multi-dither [4–8], single-dither [9,10], the code division multiplexing based DEHI and hybrid systems combining multiple methods [11,12].

#388381 https://doi.org/10.1364/OE.388381
Journal © 2020 Received 16 Jan 2020; revised 11 Mar 2020; accepted 13 Mar 2020; published 25 Mar 2020

Optics EXPRESS

Multiple-frequency dithering works by modulating the phase of each emitter with a unique low modulation depth radio-frequency. This allows the relative phase of emitter-pairs to be isolated via coherent demodulation. A leading example of multiple-frequency dithering is Locking of Optical Coherence by Single-detector Electronic frequency Tagging (LOCSET) [4]. Single-dither rapidly alternates the dither between each emitter, analogous to a form of time-division multiplexing.

A key benefit of DEHI is the use of auto-correlating PRBS such as M-sequences enables the isolation of optical fields based on time-of-flight. Separating signals based on time-of-flight can suppress unwanted inline reflections that can occur in fiber systems or reflections from the far-field in the case of an OPA. It should be noted that range-resolved interferometric measurements have also been processed using a sinusoidal frequency modulation [13]. For a given application, M-sequences could also be exchanged with a sequence with different cross- and auto-correlation properties such as those studied and employed in radio-frequency communications [14].

Variations of DEHI have found applications in multiplexed optical displacement measurements for satellite interferometry and audio sensing [15,16], optical fiber frequency references [17], optical frequency domain reflectometry [18], 2D wavefront sensing [19], and optical phased arrays [20,21]. The technique can also be useful in applications that benefit from the rejection of unwanted in-line reflections or Rayleigh scattering [22].

Similar to radio-frequency CDMA (code division multiple access), crosstalk is dependent on the number of signals and can degrade the quality of the measurement [23]. The term crosstalk is used in this work to describe any contribution to the desired phase measurement from signals other than the one targeted. Crosstalk is of particular relevance to applications which require a large number of signals such as OPAs or those which involve signals with asymmetric power ratios such as satellite interferometry.

In this paper, the influence of crosstalk when using Digitally Enhanced Heterodyne Interferometry to measure the phase of optical fields is explored. In Section 2, an analytical representation of crosstalk is presented, exploring its dependence on the quantity, magnitude and relative phase of input optical fields. In Section 3, an experimental implementation of DEHI is used to investigate practical effects and parameter choices which significantly influence crosstalk, particularly when scaling to more channels. This includes misaligned chip transitions, bandwidth limitations for PRBS modulation, choice of heterodyne frequency, crosstalk frequency, relative phase between multiple suppressed channels and the large potential contribution from homodyne components of the signal. Section 4 discusses the expected performance and limitations when scaling to hundreds or more channels.

2. Origin of crosstalk

2.1. Electric fields

The structure of a DEHI setup in the form of a fiber Mach-Zehnder interferometer, able to measure multiple optical paths, is shown in Fig. 1. Light is separated into two arms with a beamsplitter. One arm, designated the local oscillator (LO), is frequency-shifted using an acousto-optic modulator (AOM). The other arm, designated the signal arm, can vary depending on the required application. The common features required in a signal arm is the generation of multiple electric fields, each with a different delay (or different sequence) of phase encoded PRBS. Each optical path with a differently delayed PRBS is referred to as a channel. The signal arm configuration shown in Fig. 1 generates each channel using different fiber delays, however the technique is equally compatible with a signal arm that has an individual phase modulator in each channel or multiple free-space reflections. Generating different delays by adding physical fiber lengths will increase fiber phase noise as well as laser frequency noise, which can be avoided by using individual phase modulators with path-length matched arms (as used in the later experiment).

Optics EXPRESS

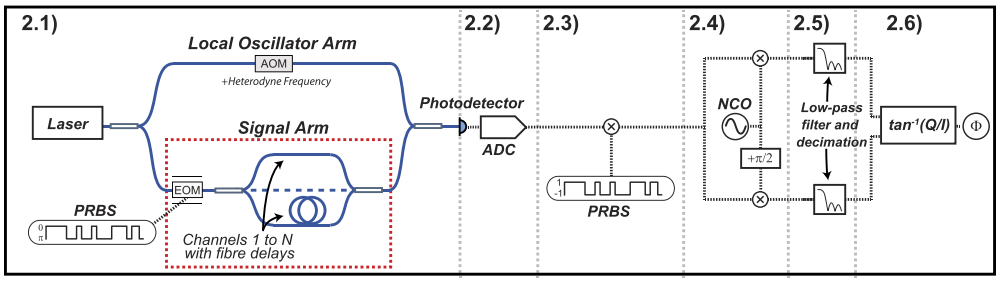

Fig. 1. Layout of an optical setup and key signal processing steps for a N-channel optical phase sensor using DEHI. Each step: 2.1, 2.2, 2.3, 2.4, 2.5 and 2.6 correspond to the electric fields interference, signal detection, PRBS decoding, Quadrature demodulation (using numerically controlled oscillator (NCO), Signal filtering/decimation and Phase readout sections. The signal arm shown (highlighted by the red box), separates channels based on fiber delays.

The electric field at the photodetector is the sum of the local oscillator field and all of the signal fields:

$$E_{PD} = E_{LO}e^{i(\omega_{LO}t+\phi_{LO})} + \sum_{n=1}^{N} E_n e^{i(\omega_n t+\phi_n+\beta c(t-\tau_n))} \tag{1}$$

The first term in Eqn. 1 represents the electric field of the frequency shifted local oscillator (LO) with amplitude E_{LO}, angular frequency ω_{LO}, and optical phase ϕ_{LO}. The second term represents the summation of N PRBS-encoded electric fields originating from the signal arm with amplitude E_n, frequency ω_n, optical phase ϕ_n, and PRBS $\beta c(t-\tau_n)$. A heterodyne frequency, ω_{het} is defined as $\omega_{LO} - \omega_n$. For the PRBS, β represents the modulation depth, τ_n represents the delay of each sequence relative to a reference at the detector and $c(t) \in [0, 1]$ is the pseudo-random sequence. For brevity, $c(t-\tau_n)$ is represented by c_n. Amplitudes are defined at the photodetector which are attenuated compared to the electric fields within the arms prior to recombination. The following signal processing steps isolate and measure the optical phase from a single channel, ϕ_i.

2.2. Signal detection

A photodetector converts the interfering electric fields into a measurable voltage signal proportional to $s_{PD} = E_{PD}E^*_{PD}$. This photodetector signal is converted to a discrete-time waveform using a single analog-to-digital converter (ADC) with sampling rate, f_s. The conversion from Watts to Volts is accounted for by a change of variable, i.e. $E_{LO} \rightarrow A_{LO}$. The digitized signal can be expressed as the sum of three components.

$$s_{PD} = s_{DC} + s_{het} + s_{hom} \tag{2}$$

The first components are DC terms, s_{DC} shown in Eqn. 3a. In practice, the DC component can limit the dynamic range of the ADC and can be removed using a high-pass filter or AC-coupled photodetector. The remaining components are a collection of beatnotes from the interference of each field with every other field. The second components are the heterodyne beatnotes from the interference of the local oscillator and each signal arm electric field, s_{het} in Eqn. 3b. The third components are the homodyne beatnotes originating from the interference of each channel with each other channel from the signal arm, s_{hom} in Eqn. 3c.

$$s_{DC} = A^2_{LO} + \sum_{n=1}^{N} A^2_n \tag{3a}$$

Optics EXPRESS

$$s_{het} = \sum_{n=1}^{N} 2A_{LO}A_n \cos\left(\omega_{het}t + \phi_{LO} - \phi_n - \beta c(t - \tau_n)\right) \tag{3b}$$

$$s_{hom} = \sum_{m=1}^{N-1} \sum_{n=1}^{N-m} 2A_nA_{n+m} \cos\left((\phi_n - \phi_{n+m}) + \beta c(t - \tau_n) - \beta c(t - \tau_{n+m})\right) \tag{3c}$$

Each of the beatnotes can be described as a combination of encoded and unencoded components weighted by the modulation depth:

$$\cos\left(\phi + \beta c(t - \tau)\right) = \underbrace{\sin\left(\frac{\beta}{2}\right)\sin\left(\phi + \frac{\beta}{2}\right)p(t - \tau)}_{\text{Encoded Component}} + \underbrace{\cos\left(\frac{\beta}{2}\right)\cos\left(\phi + \frac{\beta}{2}\right)}_{\text{Unencoded Component}} \tag{4}$$

Where $p(t)$ is the bipolar version of the sequence according to: $p(t) = 1 - 2c(t) \in [1, -1]$.

2.3. PRBS decoding

The total waveform, s_{PD}, is multiplied with a time delayed version of the PRBS matching the delay of a single heterodyne beatnote, τ_i. This decodes the beatnote containing $\phi_{LO} - \phi_i$ and re-encodes all others. The multiplication of two M-sequences is given by [24]:

$$p(t - \tau_i) \cdot p(t - \tau_j) = \begin{cases} 1 & \text{if } i = j : \text{Correctly Decoded} \\ p(t - \tau_k) & \text{if } i \neq j : \text{Incorrectly Decoded} \end{cases} \tag{5}$$

Where τ_i, τ_j and τ_k are three different delays applied to the same sequence. The intrinsic range-gate enabled by the sequence in fiber, d_{min} is governed by the frequency of transitions between bits of the sequence referred to as the chip frequency, f_{chip}. This is given by:

$$d_{min} = \frac{c}{n_{fiber}f_{chip}} \tag{6}$$

Where n_{fiber} is the refractive index of the fiber. Additional noteworthy parameters relating to the PRBS referred to in this work are the codelength, L which is the non-repeating length of the sequence (in chips) and the code frequency, $f_{code} = \frac{f_{chip}}{L}$ which is the repetition rate of the entire code (in Hz).

2.4. Quadrature demodulation

The phase of the correctly decoded heterodyne beatnote is extracted using a phase measurement algorithm such as Quadrature demodulation which performs an arctangent on the In-Phase and Quadrature components of a signal at a given heterodyne frequency. For applications requiring low latency phase measurements, a phase-locked loop system can be used [25,26]. The first stage in generating In-phase and Quadrature components of the decoded heterodyne beatnote is to digitally duplicate the decoded ensemble, then mix with 90 degree phase shifted numerically controlled oscillators at the heterodyne frequency. This generates the mixed signals, M_I and M_Q

$$M_I = s_{PD}p_i \sin\left(\omega_{het}t + \phi_{NCO}\right) \tag{7a}$$

$$M_Q = s_{PD}p_i \cos\left(\omega_{het}t + \phi_{NCO}\right) \tag{7b}$$

This operation generates two components for each of the beatnotes present (including those incorrectly decoded and originating from homodyne interference between signal arm fields).

Optics EXPRESS

One is downshifted in frequency by ω_{het} and another upshifted in frequency by ω_{het}. Each signal present after Quadrature demodulation has the common form shown in Eqn. 8.

$$A \sin(\omega t + \phi(t))P \tag{8}$$

Where, A is the amplitude of the signal, ω is the frequency of the signal, $\phi(t)$ is the phase of the signal, and P represents the multiplication of PRBS present for each signal. A summary of the number and parameters of signals contributing to M_Q is given in Table 1. These signals are categorized and given a descriptor based on their origin. s_{het} and s_{hom} refer to whether the signal originated from the interference between the local oscillator and signal fields or between signal fields and signal fields. The arrows refer to whether they are the downshifted or upshifted components and the asterisk ($*$) denotes the correctly decoded signal. The M_I version of the signal can be described by applying a 90 degree phase shift to each listed signal.

Table 1. Parameters for each signal comprising M_Q. The first row contains the correctly decoded signal and the remaining rows are the signals contributing to crosstalk

Target Signal					
Origin	Quantity	A	ω	ϕ	P
$s_{het} \downarrow *$	1	$-A_i A_{LO} \sin\left(\frac{\beta}{2}\right)$	0	$\phi_{LO} - \phi_i - \phi_{NCO}$	1
Crosstalk Signals					
Origin	Quantity	A	ω	ϕ	P
$s_{het} \downarrow$	N-1	$-A_n A_{LO} \sin\left(\frac{\beta}{2}\right)$	0	$\phi_{LO} - \phi_n - \phi_{NCO}$	$p_n p_i$
$s_{het} \uparrow *$	1	$-A_i A_{LO} \sin\left(\frac{\beta}{2}\right)$	$2\omega_{het}$	$\phi_{LO} - \phi_i + \phi_{NCO}$	1
$s_{het} \uparrow$	N-1	$-A_n A_{LO} \sin\left(\frac{\beta}{2}\right)$	$2\omega_{het}$	$\phi_{LO} - \phi_n + \phi_{NCO}$	$p_n p_i$
$s_{hom} \downarrow$	$\frac{N^2-N}{2}$	$A_n A_{n+m} \sin^2\left(\frac{\beta}{2}\right)$	$-\omega_{het}$	$\phi_n - \phi_{n+m} - \phi_{NCO} + \frac{\pi}{2}$	$p_n p_{n+m} p_i$
$s_{hom} \uparrow$	$\frac{N^2-N}{2}$	$A_n A_{n+m} \sin^2\left(\frac{\beta}{2}\right)$	ω_{het}	$\phi_n - \phi_{n+m} + \phi_{NCO} + \frac{\pi}{2}$	$p_n p_{n+m} p_i$

It should be noted that Table 1 corresponds to the modulated component of each signal and it is assumed that each signal arm has the same modulation depth, β. The unmodulated components present with a reduced modulation depth could be described using the weighting and phase shifted described in Eqn. 4.

2.5. Signal filtering and decimation

A low pass filter (LPF) is required to attenuate all except the first row of Table 1, which is possible since all other signals have either $\omega \neq 0$, or are still encoded with a PRBS. However, the wide frequency range of PRBS encoded signals means extra consideration needs to be given to their filtering compared to a single high frequency harmonic.

In the frequency domain, the power of each incorrectly decoded signal is spread by the convolution with the PRBS. The resultant spectra consists of periodic harmonics with an approximately *sinc* amplitude envelope, with each PRBS harmonic carrying the spectral characteristics of the incorrectly decoded signal's optical phase, $\phi_n(t)$. This envelope has nulls at the chip frequency, f_{chip} and is centred at the frequency corresponding to the ω column of Table 1 for each signal. The harmonics occur at integer multiples of f_{code}. The frequency spectrum of a PRBS encoded signal, mathematically described by Eqn. 8, using an M-sequence 15 chips in length is shown in Fig. 2(a).

Optics EXPRESS

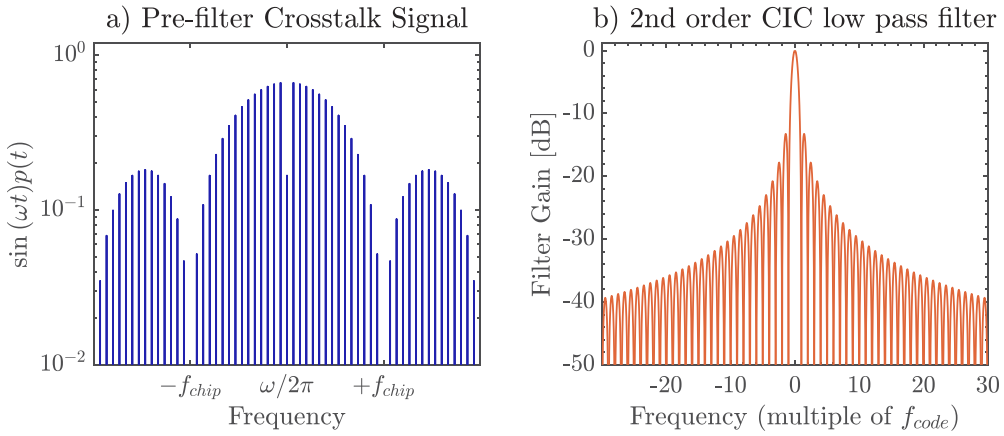

Fig. 2. a) Frequency spectrum of a signal encoded with 15 chip length PRBS and b) Magnitude Response of a 2nd order CIC filter with decimation set to the period of the PRBS. When the filter decimation is set to the code frequency, the spacing of filter nulls matches PRBS harmonic spacing.

Moving average low pass filters with decimation, such as a Cascaded Integrating Comb (CIC) filter or a "Sum and Dump" filter, have properties convenient for removing these types of signals. Namely, the filters have periodic nulls which can be aligned to the position of the PRBS harmonics in addition to a roll-off at high frequencies. The gain profile of a CIC filter is shown in Fig. 2(b).

Aligning the spacing of the filter nulls to the PRBS harmonics to remove the high frequency harmonics is achieved by setting the filter decimation, R, to the number of digital samples in a complete period of the code, given in Eqn. 9, where L is the previously defined codelength and $\frac{f_s}{f_{chip}}$ is the number of digital samples per chip.

$$R = L\frac{f_s}{f_{chip}} \tag{9}$$

Quantitatively, the magnitude response of a CIC filter of order M, acting on a sine wave at frequency, f, can be approximated by Eqn. 10.

$$H_{CIC:Mth}(f) \approx \left(\frac{f_s}{\pi f}\sqrt{\sin^2\left(\frac{\pi R f}{f_s}\right)}\right)^M \tag{10}$$

An important property for these filters is the reduction in sampling rate by a factor equal to the decimation which decides the bandwidth of the phase measurement. The condition in Eqn. 9 results in a decimated rate of f_{code} and a measurement bandwidth half of this given by:

$$\textit{Measurement Bandwidth} = \frac{f_s}{2R} = \frac{1}{2}f_{code} = \frac{1}{2}\frac{f_{chip}}{L}(\text{Hz}) \tag{11}$$

In general, the crosstalk is from the remnant of each PRBS encoded signal after filtering which will be a harmonic in the measurement band with potential contributions from higher frequency harmonics aliasing into the measurement band. The magnitude of this quantity is represented by η. For an ideal signal, setting the heterodyne frequency equal to the chip frequency will cause the null of the PRBS spectra to be shifted to the measurement band for the $s_{het}\uparrow$ and s_{hom} crosstalk signals. In this case, the only remaining crosstalk would be from $s_{het}\downarrow$ signals, having magnitude equal to $1/L$ - matching the autocorrelation property of M-sequences. The frequency spectra

Optics EXPRESS

of the crosstalk in each frequency regime are displayed in Fig. 3. Whether this is practically achievable is explored in the following sections.

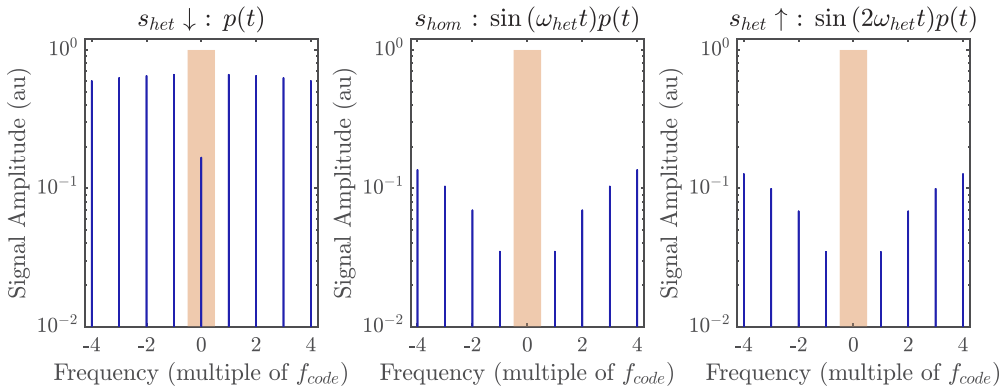

Fig. 3. Frequency spectra around DC representing the three categories of crosstalk signals when the heterodyne frequency is equal to the chip frequency and a 4-bit PRBS. This results in a PRBS spectrum null centred in the shaded measurement band for the $s_{het} \uparrow$ and s_{hom} signals which should remove crosstalk from these signals. The harmonic in the measurement band for $s_{het} \downarrow$ signals is equal to $1/L$ which is the DC average of an M-sequence PRBS.

In addition to altering the amplitude of the signal, there may be a phase shift of the filtered signal originating from the combined phase of the contributing PRBS harmonics and the CIC filter, denoted by, ϕ_{p_n}. For the DC harmonic of the PRBS, $\phi_{p_n} = \pi$ due to having one more -1 than 1 in the M-sequence.

2.6. Phase readout

The final stage of the phase measurement performs an arctangent operation on the filtered In-Phase and Quadrature signals, denoting the filtered versions by I and Q. The phase corresponding to the $s_{het} \downarrow$ signals when decoding channel i is given in Eqn. 12 using the substitutions, $\Phi_i = \phi_{LO} - \phi_i - \frac{\beta_i}{2} - \phi_{NCO}$ and $\Phi_n = \phi_{LO} - \phi_n - \frac{\beta_n}{2} - \phi_{NCO} + \phi_{p_n}$. This subset of crosstalk signals are included as they potentially have the largest residual. If other crosstalk signals are not sufficiently suppressed they would also need to be added.

$$\begin{aligned}\Phi &= \tan^{-1}\left(\frac{Q}{I}\right) \\ &= \tan^{-1}\left(\frac{LA_{LO}A_i \sin(\Phi_i) + A_{LO}\sum_{n=1;n\neq i}^{N} A_n\eta_n \sin(\Phi_n)}{LA_{LO}A_i \cos(\Phi_i) + A_{LO}\sum_{n=1;n\neq i}^{N} A_n\eta_n \cos(\Phi_n)}\right)\end{aligned} \tag{12}$$

Where η_n is the suppression factor from low pass filtering the PRBS encoded signals. To better evaluate how the suppressed phase signals contribute to the targeted phase signal, a shared phase rotation of all signals by Φ_i allows the targeted phase to be separated in the form:

$$\Phi = \Phi_i + \tan^{-1}\left(\frac{\sum_{n=1,n\neq i}^{N-1} \frac{\eta_n}{L}\frac{A_n}{A_i} \sin\left(\phi_i(t) - \phi_n(t) + \phi_{p_n}\right)}{1 + \sum_{n=1,n\neq i}^{N-1} \frac{\eta_n}{L}\frac{A_n}{A_i} \cos\left(\phi_i(t) - \phi_n(t) + \phi_{p_n}\right)}\right) \tag{13}$$

Further simplification can be achieved using that when $\frac{\eta_{\Sigma:DC}}{L}\frac{A_n}{A_i} \ll 1$, the +1 dominates the denominator followed by the small angle approximation for arctangent.

$$\Phi = \Phi_i + \sum_{n=1,n\neq i}^{N-1} \frac{\eta_n}{L}\frac{A_n}{A_i} \sin\left(\phi_i(t) - \phi_n(t) + \phi_{p_n}\right) \tag{14}$$

Optics EXPRESS

The crosstalk will be dependent on the phase difference between the correctly decoded signal and the incorrectly decoded signal as well as their relative amplitudes. The form the crosstalk takes is analogous to the way parasitic interference from scattered light can influence a phase measurement in conventional interferometry. This has been of particular relevance in ground based gravitational wave detectors [27]. The dependence on relative amplitude may be important for some applications, particularly where a low power signal is to be isolated from a high power signal as may be the case for free space optical communication applications.

2.6.1. Phase modulated tone

In order to have a controlled phase signal when measuring crosstalk, all channels except channel 1 are phase modulated with a tone in the following experiment. A reduced amplitude version of these tones should then be measurable in the phase of channel 1. This requires a slight modification to the expression for the expected phase signal in the form of: $\phi_n(t)' \rightarrow \phi_n + \xi \sin\left(\omega_\xi t + \phi_{\xi,n}\right)$ where $\phi_n(t)$ is the "naturally" fluctuating optical phase, ω_ξ is the frequency of the tone, ξ is the modulation depth of the tone and $\phi_{\xi,n}$ is the phase of the injected tone in channel n.

The specific figure of merit for crosstalk is the measured ratio between the phase tone magnitude in channel 1, $\bar{\xi_1}$ compared to tone magnitude in channels directly modulated, $\bar{\xi_2}$. These can be measured simultaneously by splitting the ADC signal then decoding one version with $p(t-\tau_1)$ and the other with $p(t-\tau_2)$. Using full PRBS modulation depth ($\beta = \pi$), the expected measured phase for these two decoding operations are:

$$\Phi_1 = \phi_{LO} - \phi_1 - \frac{\pi}{2} + \sum_{n=1;n\neq 1}^{N} \frac{\eta_n}{L}\frac{A_n}{A_1} \sin\left(\phi_1 - \phi_n - \xi \sin\left(\omega_\xi t + \phi_{\xi,n}\right) + \phi_{p_n}\right) \tag{15a}$$

$$\Phi_2 = \phi_{LO} - \phi_2 - \xi \sin\left(\omega_\xi t + \phi_{\xi,2}\right) - \frac{\pi}{2} + \sum_{n=1;n\neq 2}^{N} \frac{\eta_n}{L}\frac{A_n}{A_2} \sin\left(\phi_2 + \xi \sin\left(\omega_\xi t + \phi_{\xi,n}\right) - \phi_n + \phi_{p_n}\right) \tag{15b}$$

The incorrectly decoded component of each signal (those weighted by η) will have harmonics at multiples of the tone frequency. The amplitude of these harmonics are given by Bessel functions of the first kind and can be expanded using the identity:

$$\sin\left(\xi \sin\left(\omega t + \phi\right)\right) = 2\sum_{n=1}^{\infty} J_{2n-1}\left(\xi\right) \sin\left((2n-1)(\omega t + \phi)\right) \tag{16}$$

Using this identity, the amplitude of the phase signals at ω_ξ (the J_1 components) for each phase measurement, $\bar{\xi_1}$ and $\bar{\xi_2}$ can be isolated and the ratio for suppression of crosstalk calculated. This uses that when ξ is small, $2J_1(\xi)/\xi \approx 1$.

$$\begin{aligned}\frac{\bar{\xi_1}}{\bar{\xi_2}} &= \frac{-\sum_{n=1;n\neq 1}^{N} \frac{\eta_n}{L}\frac{A_n}{A_1} \cos\left(\phi_1(t) - \phi_n(t) + \phi_{p_n}\right) 2J_1(\xi)}{\xi + \sum_{n=1;n\neq 1}^{N} \frac{\eta_n}{L}\frac{A_n}{A_2} \cos\left(\phi_2(t) - \phi_n(t) + \phi_{p_n}\right) 2J_1(\xi)} \\ &\approx \sum_{n=1;n\neq 1}^{N} \frac{\eta_n}{L}\frac{A_n}{A_1} \cos\left(\phi_1(t) - \phi_n(t) + \phi_{p_n}\right)\end{aligned} \tag{17}$$

For two channels, provided the injected tone is the dominant signal source at the tone frequency, the expected crosstalk suppression ratio for this experiment is:

$$\frac{\bar{\xi_1}}{\bar{\xi_2}} \approx \frac{\eta_2}{L}\frac{A_2}{A_1} \cos\left(\phi_1(t) - \phi_2(t) + \phi_{p_2}\right) \tag{18}$$

In the experimental system presented in this work, no feedback is applied to stabilize the optical phase difference. This should result in a randomly distributed optical phase difference that with

Optics EXPRESS

sufficient averaging, will cause the absolute value of the term; $\cos\left(\phi_1(t) - \phi_2(t) + \phi_{p_2}\right)$ to average to approximately 0.6366.

For systems with more than two channels, the phase difference between the injected tones, $\phi_{\xi,n}$ will affect the addition of each signal contributing to crosstalk. That is, whether the incorrectly decoded signals add constructively or destructively at the tone frequency. If the phase of each channel at a given frequency is uncorrelated, the amplitude of the incorrectly decoded signals should be added in quadrature.

3. Practical suppression of DEHI crosstalk

An experimental DEHI system was setup to investigate the crosstalk from suppressed channels into a targeted channel's phase measurement. There are three stages of the experiment. Firstly, to characterize the difference between the analytically described "ideal" PRBS encoded signal and an experimental PRBS encoded fiber based signal. Secondly, to measure the crosstalk from a single suppressed channel and explore parameters on which this crosstalk depends. Finally, to measure the scaling of crosstalk as the number of channels added to the signal arm increases. Numerical simulation accompanies the experimental results as needed for isolating individual effects.

3.1. Setup

The layout of the experimental DEHI tests is shown in Fig. 4. Different configurations of the signal arm are implemented to test different effects. The first configuration is used for the characterization of the PRBS modulation. The second configuration measures the crosstalk between two channels. The final configuration iteratively adds four more channels to the signal arm to investigate the scaling of crosstalk.

In the optical section of this setup, an Nd:YAG non-planar ring oscillator laser operating at 1064 nm was split into local oscillator and signal arms using a free space polarizing beam splitter. The beam in both paths was passed through a half waveplate and polarizing beam splitter to control the power in the local oscillator and signal arm. The optical power at the photodetector from the local oscillator was 10 μW, and 1 μW from channel 1. The local oscillator to signal arm power ratio was skewed towards to the local oscillator to reduce the magnitude of the s_{hom} terms. The overall power level was limited by saturation of the photodetector when all channels were present in the signal arm.

Each beam was then double passed through an acousto-optic modulator (AOM), generating a controllable heterodyne frequency, $\frac{\omega_{het}}{2\pi} = f_{het} = 2\left(f_{LO} - f_{sig}\right)$. The double pass was performed using a "cat's eye" retro-reflector setup to increase range of heterodyne frequencies. A quarter waveplate is included in the retro-reflected path to cause the reflected beam to exit from reflection port of the beam splitter. Both arms were launched into polarization maintaining fiber (PM980). Once in fiber, the local oscillator was left unmodified until recombination with the signal arm. The composition of the signal arm varies depending on the targeted measurement, with each signal arm configuration described as it arises. However in general, delayed PRBS are directly modulated onto each channel rather than using delay lines. The PRBS was an M-sequence with $f_{chip} = 20$ MHz (chip frequency) generated on an FPGA using a linear feedback shift register (LFSR) with k bits, corresponding to a sequence length of $L = 2^{k-1}$ chips. As such, the codelength can also be described in terms of these bits, e.g. a 6-bit code has $L = 63$.

The optical fields from the local oscillator and signal arms were recombined and passed through a variable fiber attenuator before incidence on an Newport 1811-FC InGaAs AC-coupled photodetector with a 125 MHz bandwidth. The analog electronic signal from the photodetector was digitized with a 16-bit analog-to-digital converter, sampling with $f_s = 80$ MHz. The digitized signal was processed using an NI-7854R Field Programmable Gate Array (FPGA). This FPGA also generated the voltage signals sent to the EOMs for the phase tone and individually

Optics EXPRESS

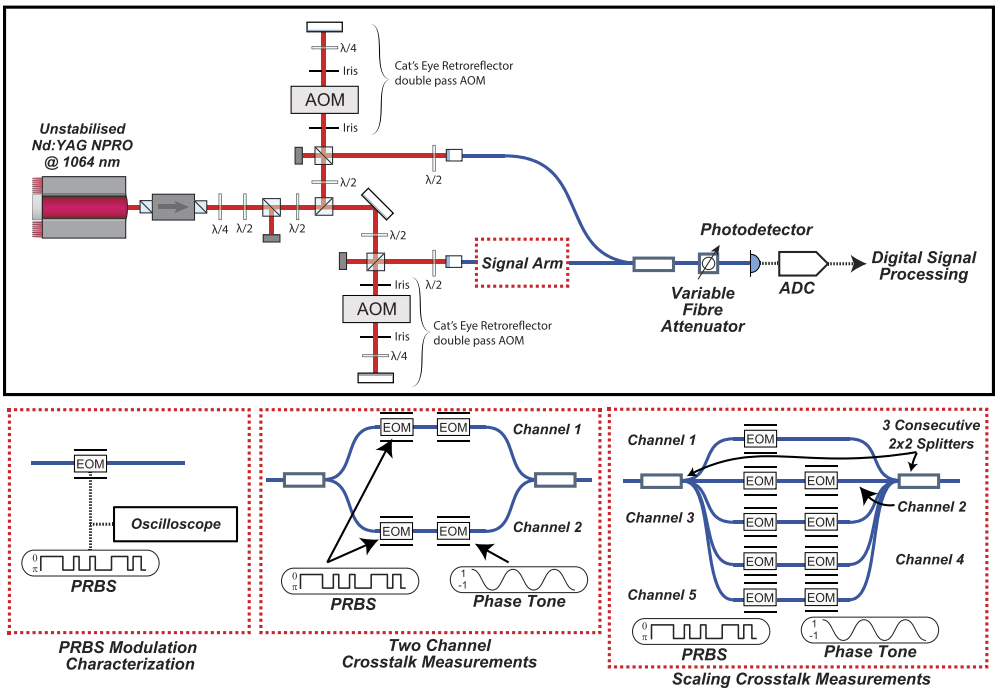

Fig. 4. The experimental heterodyne Mach-Zehnder interferometer used for the investigation of crosstalk when multiplexing optical phase signals using DEHI. Three different signal arm configurations are outlined, used for different measurements.

delayed PRBS using the 1 MS/s analog outs and digital outs with a 12.5 ns minimum pulse (80 MHz) respectively. As the encoding and decoding PRBS are both generated on the same FPGA, they are intrinsically phase-locked, while the signal generator used to seed the AOM was phase-locked using the equipment's 10 MHz reference clock. The PRBS decoding and Quadrature demodulation (including filtering) signal processing was performed on the FPGA. This generated the In-phase and Quadrature data at the code frequency, f_{code} which varied with different codelengths, up to $\approx$ 150 kHz. The In-phase and Quadrature data was saved by transferring the data to a CPU sharing a chassis with a hard drive. Once saved, the phase was calculated using an arctangent followed by a phase unwrapping algorithm in post-processing.

3.2. PRBS modulation characterization

3.2.1. PRBS modulation bandwidth

Unlike the analytically described system, the experimental generation and modulation of the PRBS is subject to the finite bandwidth of the equipment, primarily the digital outs, electronic amplifiers and electro-optic modulators, previously suspected of reducing the achievable range-gate [28]. To check the generation of the PRBS and implications of finite bandwidth on the achievable crosstalk suppression, a time domain recording of the electronic PRBS signal prior to the EOM and power spectrum measurement of the encoded optical beat-note are shown in Fig. 5. A relatively short (6-bit) sequence was used in order to clearly identify individual harmonics.

The time domain plot of the PRBS voltage signal before the EOM shows the varying bit transition spacing for a 20 MHz chip frequency code (minimum of 50 ns), with overshoots at the bit transitions characteristic of low pass filtering. Any impedance mismatch between the

Optics EXPRESS

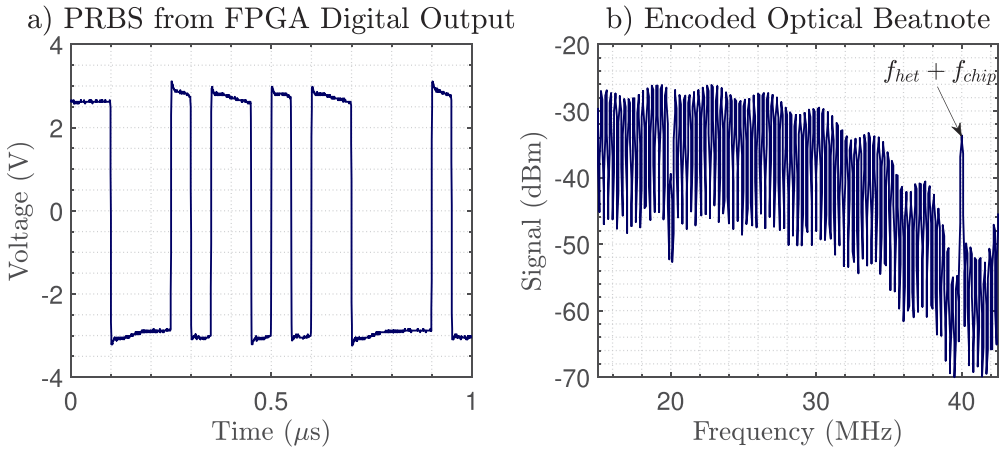

Fig. 5. Bandwidth effects on an experimental PRBS modulation generated by the FPGA's digital outputs. a) A time domain measurement of the 20 MHz PRBS voltage signal applied to the electro-optic modulators showing the chip transition overshoots characteristic of bandwidth limitations. b) A section of the power spectrum of the PRBS encoded optical heterodyne beatnote measured on the photodetector showing a spike positioned at $f_{het} + f_{chip}$ not present in the simulated frequency spectrum of a "pristine" PRBS (e.g. Figure 2).

digital source and EOMs could also result in reflections of the electronic PRBS signal producing a similar, compounding effect.

Once encoded onto the beatnote, the characteristic spread spectra shape is apparent, however there is a significant harmonic at 40 MHz in place of the desired spectrum null. Addition spikes were positioned at multiples of the chip frequency centred around the heterodyne frequency, mathematically described by: $nf_{chip} \pm (f_{chip} - f_{het})$. The location of these spikes is particularly relevant to the suppression of the crosstalk signals s_{hom} and $s_{het}\uparrow$ which relied on the null of the PRBS spectra for their suppression. Additionally, because this effect is dependent on chip transitions (rather than the overall code length), the amplitude of the spikes can't be reduced by increasing codelength. It is not known whether the ≈4 MHz ripple on the overall spectra was caused by filtering of the PRBS or a result of the frequency spectrum calculation settings across the broad band.

In regard to minimizing imperfect PRBS modulation, removing reflections in the electronics from an impedance mismatch can be achieved by changing the electronic setup (or adding in line attenuators). However, bandwidth limits can be difficult to avoid in practice, particularly when operating at high speeds. Reducing the impact bandwidth limits are expected to have on crosstalk could be achieved by reducing the chip frequency (at the cost of a reduced measurement bandwidth) or through the use of improved electronics. Another change to partially mitigate this effect is to shift the heterodyne frequency by f_{code}, such that $f_{het} = f_{chip} - f_{code}$. The spikes for the $s_{het}\uparrow$ signals should then end up in one of the LPF nulls and the smaller adjacent harmonics will appear in the measurement band. In this work, it is believed that the digital outs on the FPGA are the bandwidth limiting component.

3.2.2. Digital samples per chip

We now consider the number of digital samples per chip of the PRBS and how it affects the aliasing of the entire spectra after digitally sampling the photodetector signal. Figure 6 shows a simulated frequency spectra of digitally sampled shifted PRBS signals for the s_{hom} and $s_{het}\uparrow$

Optics EXPRESS

components of the crosstalk with four, two and one samples per chip. The specific versions plotted have set $f_{het} = f_{chip}$.

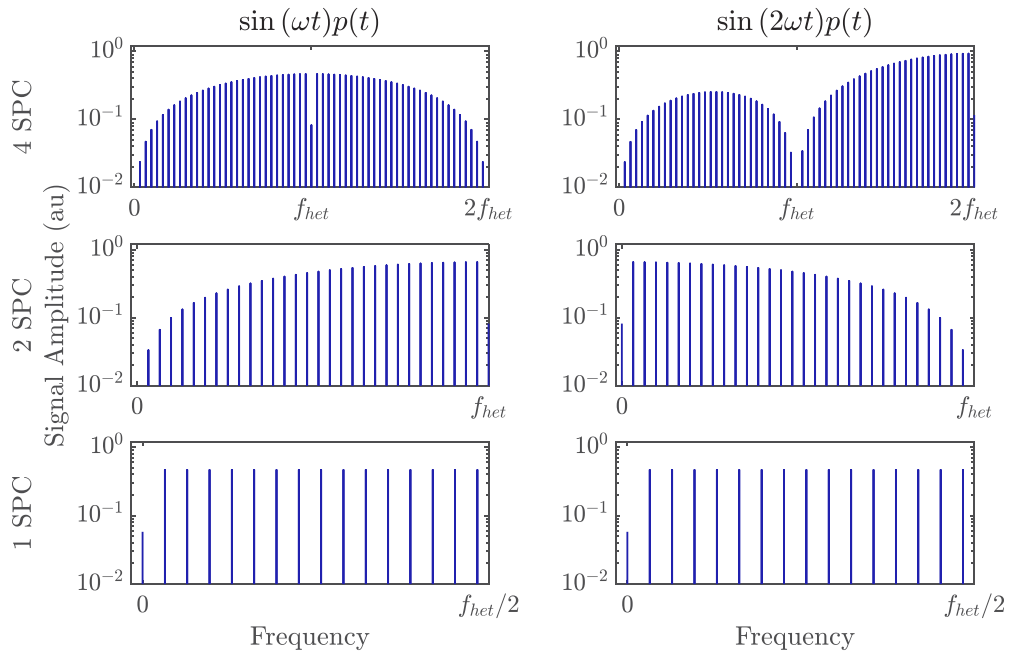

Fig. 6. Simulated frequency spectra of PRBS encoded sinusoids representing of s_{hom} (left) and $s_{het}\uparrow$ (right) signals with four, two and one samples per chip (SPC). With a reduced number of samples per chip, the spectra loses the characteristic sinc shape as well as the null centred at DC.

When digitally sampled such that there are four samples per chips, the overall PRBS shape is maintained for both cases, reproducing the null in the measurement bandwidth required for maximum crosstalk suppression. With two samples per chip, the higher frequency harmonics in the $s_{het}\uparrow$ case alias such that there is a non-zero harmonic in the measurement band. In the single sample per chip case, this occurs for both $s_{het}\uparrow$ and s_{hom} signals. As a result, the non zero harmonics in the measurement band for these signals will be expected to increase crosstalk when having less than four samples per chip. Increasing the number of samples per chip by decreasing the chip frequency has a trade-off in the form of a larger range gate which limits the ability to resolve signals with similar delays.

3.2.3. Subchip delays

Ideally, the relative delay of the digitally sampled input signal's PRBS and the digital PRBS used for decoding would be restricted to an integer numbers of chips. Experimentally however, different optical pathlengths and electronic delays may result in fractional offsets, referred to as subchip delays. A visualization of integer chip aligned and subchip offset PRBS multiplication is shown in Fig. 7 for a subsection of an M-sequence to illustrate this effect.

When the two PRBS signals are delayed by an integer number of chips, the result is a differently delayed version of the sequence with the same sampling properties. When one PRBS is offset by a fractional delay, the product of the PRBS can be considered as the combination of two adjacently delayed M-sequences, with different sampling frequencies. Each of these PRBS components may not be getting sufficiently sampled, i.e. there are less than four samples per chip.

Optics EXPRESS

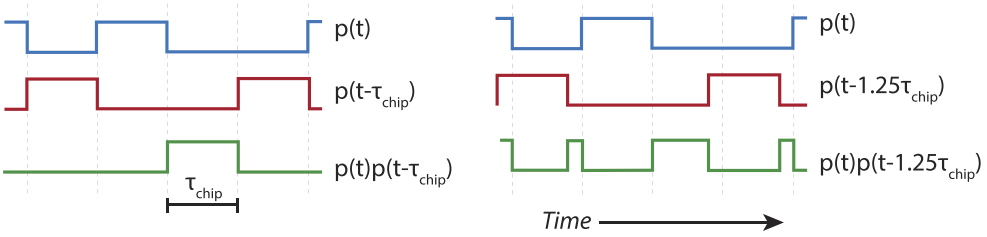

Fig. 7. Multiplication of two differently delayed PRBS. a) Aligned chip transitions where the PRBS are separated by an integer chip delay (τ_{chip}), producing another PRBS with the same chip frequency. b) Mis-aligned chip transitions where the two PRBS are separated by a fractional delay, resulting in the appearance of shorter, higher frequency chips.

The potential impact of mis-aligned chip transitions can be observed based on the spectra of the signal in the frequency domain. The frequency spectrum of the signal resulting from multiplications of PRBS separated by subchips were simulated and are shown in Fig. 8.

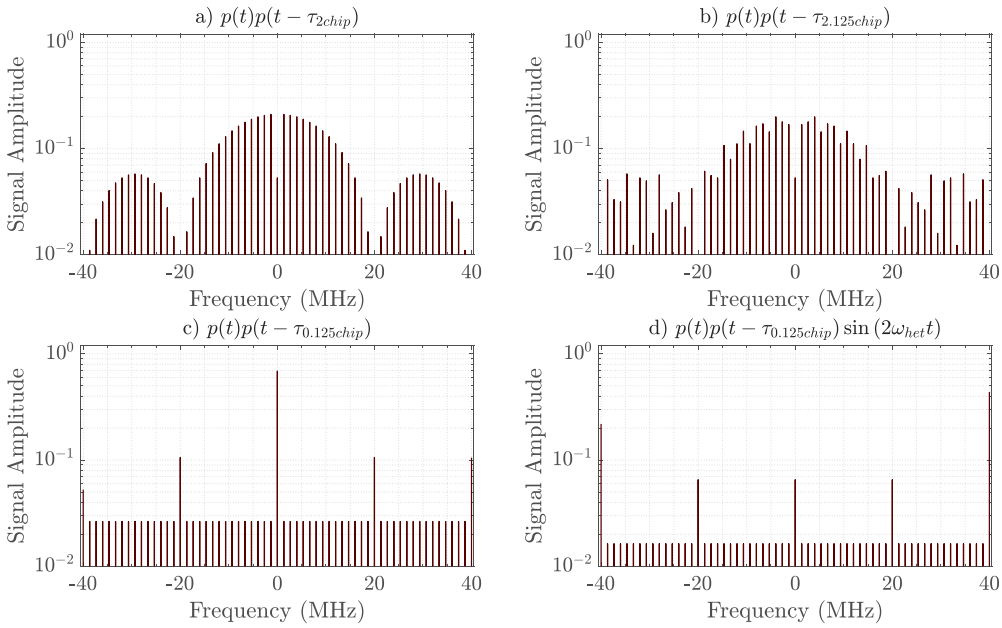

Fig. 8. Simulated frequency spectra of the product of subchip delayed decoding PRBS with four samples per chip. a) Two PRBS are separated by integer chip delays producing the ideal spectrum. b) Two PRBS separated by a fractional delay. This changes the height of many of the PRBS harmonics which could cause a varying amount of crosstalk for configurations where f_{het} is not equal to the chip frequency. c) Two PRBS separated by less than a chip displays a combination of a decoded signal (large spike at DC) and a spread spectrum (across the entire frequency range). There are also spikes at multiples of the chip frequency which could reduce suppression of $s_{het}\uparrow$ if $f_{het} = f_{chip}$. d) Shows the same PRBS but modulating a signal at twice the chip frequency (representing $s_{het}\uparrow$) which shows a spike positioned in the measurement band.

As a reference, the first case shows the frequency spectrum of the product of PRBS separated by an exact number of chips, $p(t)p(t-2[\text{chip}])$ which has the same properties as the original PRBS spectra. In the second case, $p(t)p(t-2.125[\text{chip}])$, the height of each PRBS harmonics is

Optics EXPRESS

altered in comparison to the ideal spectra. This can be explained by considering that harmonics of both the differently delayed components may change in magnitude and phase, phase due to the delay change and magnitude due to aliasing. When the components of the signal are combined, these two effects result in less consistent height of the multiplied signals PRBS harmonics.

The changing of PRBS harmonic size resulting from different subchip delays is relevant to the s_{hom} and $s_{het}\uparrow$ crosstalk signals, as the PRBS harmonic in the measurement band for these signals will vary in amplitude, changing the crosstalk contribution. It is potentially more significant for the s_{hom} signals that have an additional consecutive multiplication of PRBS.

The third and fourth cases are representative of a slight misalignment of the decoding PRBS for the "correctly decoded signals", $s_{het}\downarrow *$ and $s_{het}\uparrow *$ respectively. The large signal around DC is the correctly decoded signal. The flat, lower amplitude harmonics across the whole spectra are from the incorrectly decoded component of the signal. There are also however, additional components of the signal at harmonics of the chip frequency. This is a potential issue for the suppression of the $s_{het}\uparrow *$ signal shown in the fourth case which now has a non-zero harmonic in the measurement band.

In order to reduce the impact of mis-aligned subchip delays, the same change in heterodyne frequency made to mitigate PRBS modulation bandwidth limitations could be applied, i.e. $f_{het} = f_{chip} - f_{code}$. This would result in a lower PRBS harmonic appearing in the measurement band. Having subchip control over the delay between either the experimental PRBS or the decoding PRBS could also minimize this effect.

3.3. Crosstalk between two channels

For the tests of crosstalk from one other channel, the signal arm was split into two channels, each passing through two fiber waveguide electro-optic phase modulators (EOMs). In the first channel, only a single EOM was driven with a PRBS. In the second channel, one of the EOMs modulated the PRBS, while the other added a low amplitude sinusoidal phase modulation, $f_{sig} = \frac{\omega_\xi}{2\pi} = 2$ kHz. The crosstalk was quantified by measuring the amplitude of the phase tone in both channels and converting the ratio to dB according to:

$$\text{Crosstalk} = 20\log_{10}\left(\frac{\bar{\xi}_1}{\bar{\xi}_2}\right)\text{[dB]} \tag{19}$$

Figure 9, shows the measured phase amplitude spectral density (ASD) demonstrating the difference between the original amplitude of the 2 kHz tone compared to its reduced amplitude when suppressed. Also shown is an ordinary heterodyne beatnote (i.e. with only the local oscillator and a single channel present). Comparing this to the configurations with the PRBS present, other than the injected tone and second harmonic of the tone, the noise floor remains between $1 - 10$ μcyc$/\sqrt{\text{Hz}}$ corresponding to approximately $1 - 10$ pm$/\sqrt{\text{Hz}}$ displacement sensitivity in each configuration. It is expected that the added crosstalk from sources other than the injected tone is well below the measurement sensitivity of the system.

The analytical form of the sinusoidal phase modulation tone assumed a low modulation depth. Experimentally, the depth was chosen so that if crosstalk reached the ideal suppression levels predicted analytically, the suppressed tone would still be measurable above the noise floor. At this level it is possible to see crosstalk in the higher harmonics (weighted by the Bessel-function amplitudes). For a sufficient averaging time, the systems phase fluctuations are randomly distributed and the amplitude of the crosstalk harmonics remained stable.

3.3.1. Heterodyne frequency

The choice of heterodyne frequency will shift the frequency of the $s_{het}\uparrow$ and s_{hom} signals relative to the measurement band and filter nulls. To experimentally test the influence changing the heterodyne frequency has on crosstalk, the crosstalk was measured at the different heterodyne

Optics EXPRESS

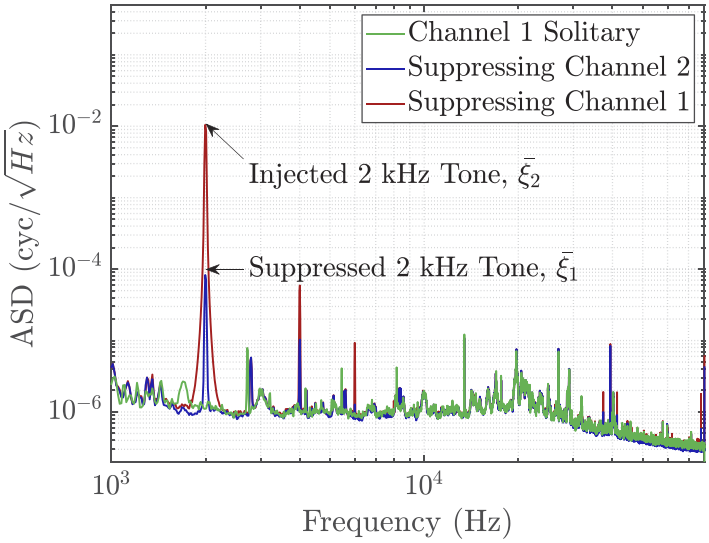

Fig. 9. Phase amplitude spectral density measurements of a 20 MHz heterodyne beatnote isolated with 7-bit PRBS demonstrating suppression of a 2 kHz tone acting as crosstalk. In green a single heterodyne beatnote without PRBS as a baseline showing no signal at 2 kHz. In red a measurement of channel 2 showing the unattenuated amplitude of the injected phase tone at 2 kHz. In blue the measurement of channel 1 while suppressing channel showing the reduced amplitude of the 2 kHz phase tone.

frequencies listed in Table 2. These heterodyne frequencies were chosen as representative cases of how changing the heterodyne frequency will affect crosstalk.

Table 2. Measured crosstalk of a 2 kHz tone for different heterodyne frequencies and a 7-bit PRBS. * See Fig. 10(a), for sensitivity to subchip delays. † See Fig. 10(b), where crosstalk is not confined to 2 kHz frequency bin

Heterodyne Description	Heterodyne Frequency [MHz]	Crosstalk at 2 kHz [dB]
$f_{het} = f_{chip}$	20.000000	−42.0*
$f_{het} = f_{chip} - f_{code}$	19.8425197	−46.0
$f_{het} = 29 f_{code}$	4.5669291	−29.6
"Misaligned"	4.500000	−41.2†

The first heterodyne frequency listed is set equal to the chip frequency, which was the ideal choice in the theorised system as it resulted in complete suppression of the crosstalk from s_{hom} and $s_{het} \uparrow$ signals. The second heterodyne frequency listed is offset by the code frequency and tests the ability to reduce the impact of bandwidth effects and mis-aligned chip transitions. The measured crosstalk was reduced when the heterodyne frequency was offset from exactly the chip frequency. Notably it was observed that macroscopic changes to the delay disproportionately affected the $f_{het} = f_{chip}$ case. This was tested by recording the crosstalk when adding different cable lengths between the photodetector and ADC. Crosstalk as a function of cable length is shown in Fig. 10(a), now using a 9-bit code ($L = 511$ chips). The increased sensitivity to pathlength and increased crosstalk is attributed to a combination of the mis-aligned chip transition effect and the spike from bandwidth limitations described in the previous sections. This supports using the $f_{het} = f_{chip} - f_{code}$ configuration which exhibited lower, more stable crosstalk.

Optics EXPRESS

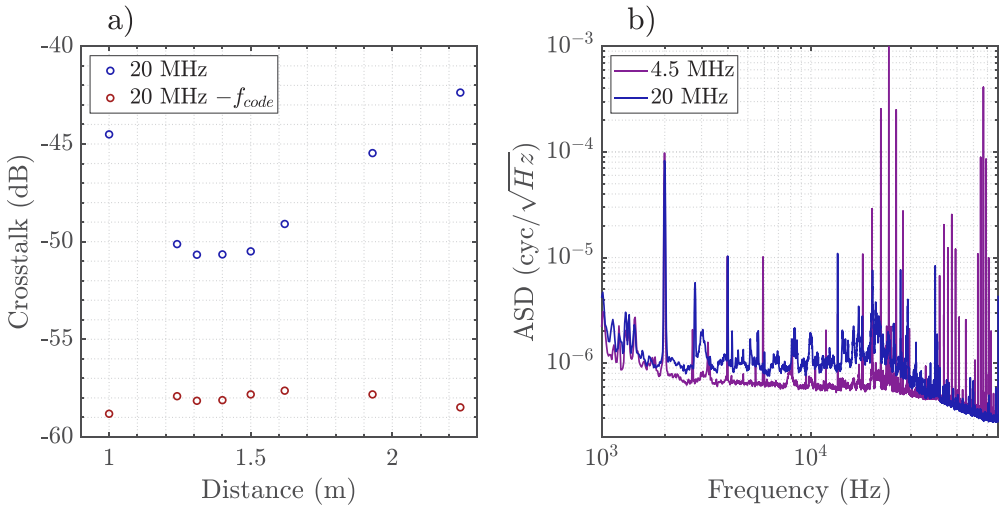

Fig. 10. a) Suppression of the 2 kHz tone when changing cable length between photodetector and ADC for the same heterodyne frequencies encoded with a 9-bit PRBS, showing an increase crosstalk and sensitivity to the subchip delay changes when $f_{het} = f_{chip}$. b) Phase amplitude spectral density of channel one's phase signal for different heterodyne frequencies $f_{het} = f_{chip}$ and $f_{het} = 4.5$ MHz. When the heterodyne frequency is not aligned to a multiple of the code frequency, multiple harmonics appear in the measurement band.

The third configuration has the heterodyne frequency set to the 29th multiple of the code frequency which is approximately a quarter of the chip frequency. In this configuration, the reduced heterodyne frequency is expected to increase the size of the harmonic in the measurement band for the s_{hom} and $s_{het}\uparrow$ terms. As a result, crosstalk from the 2 kHz tone is several times greater with the reduced heterodyne frequency.

For the first three cases, the heterodyne frequency was aligned to a multiple of the code frequency. Accordingly, the crosstalk of the 2 kHz tone appeared at 2 kHz in the measurement band in the toneless channel. The last case sets the heterodyne frequency to 4.5 MHz, which is intentionally misaligned from a multiple of the code frequency. The phase amplitude spectral density comparing the 4.5 MHz and 20 MHz heterodyne frequency configurations is presented in Fig. 10(b). While the crosstalk at 2 kHz is comparable, the 4.5 MHz heterodyne frequency case has significant signals at 23.6 kHz and 66.9 kHz each with harmonics of the 2 kHz tone attached. These frequency shifts can be predicted based on the difference between f_{het} or $2f_{het}$ and the closest multiple of the code frequency. This is generalised in Eqn. 20 which gives the frequency that different crosstalk sources should appear in the measurement band $f_{crosstalk}$, valid for values of f_{het} less than $f_s/2$.

$$f_{crosstalk} = \begin{cases} f_{sig} + 0 & \text{for } s_{het}\downarrow \\ f_{sig} + min\left(\left|H \times \frac{f_{chip}}{L} - f_{het}\right|\right) & \text{for } s_{hom} \\ f_{sig} + min\left(\left|H \times \frac{f_{chip}}{L} - 2f_{het}\right|\right) & \text{for } s_{het}\uparrow \end{cases} \quad \text{Where } H \text{ is an integer} \tag{20}$$

The lower heterodyne frequency also produces a lower broad noise floor. This is attributed to an increase in signal power with lower heterodyne frequencies due to the frequency dependence of the transmitted optical power through the AOM as well as the changing noise floor of the photodetector and ADC at different signal frequencies.

Optics EXPRESS

3.3.2. Frequency and codelength dependence of crosstalk

Physical sources of optical phase changes such as thermal and acoustic fiber noise or laser frequency noise are not confined to a single low frequency tone. Instead they are likely to be spread across the measurement band. As the frequency of optical phase changes increases, the phase noise attached to higher frequency PRBS harmonics will move out of filter nulls and towards the measurement band. To visualize how changing signal frequency will affect crosstalk, Fig. 11 shows the near measurement band frequency spectrum of a simulated PRBS encoded signal with and without small changes in frequency (representing phase noise) overlayed with the gain of a CIC filter, with decimation set by the condition in Eqn. 9. The first version has $\omega = 0$, representative of the $s_{het} \downarrow$ components where $f_{sig} \ll f_{code}$. In this case all higher frequency harmonics line up exactly with the nulls of the filter. In the second version, higher frequency PRBS harmonics no longer exactly align with the filter nulls and will have lessened suppression. The doubling of the number of harmonics is a result of the positive and negative frequency counterparts no longer being aligned.

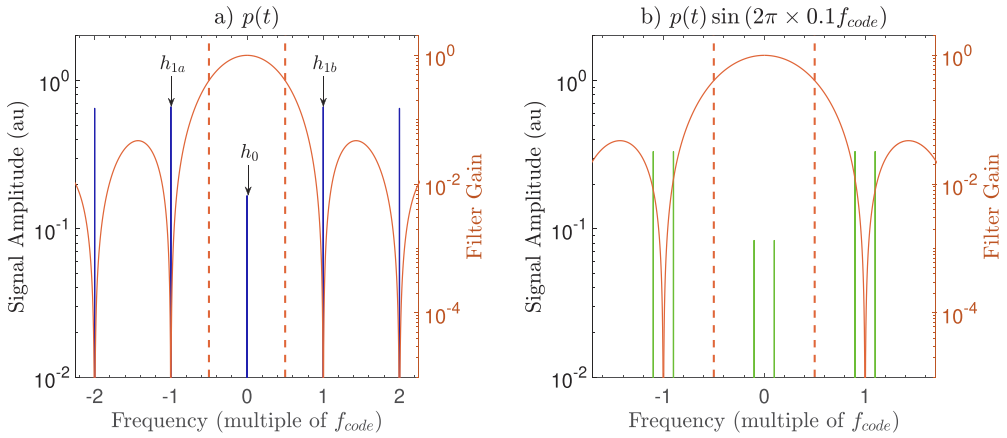

Fig. 11. Overlay of the PRBS harmonics near the measurement bandwidth with CIC filter's sinc like magnitude response for different frequency signals. a) A DC PRBS representative of $s_{het} \downarrow$ signals. b) A PRBS shifted in frequency by a fraction of code frequency ($0.1\, f_{code}$) illustrating misalignment of the filter nulls with PRBS harmonics leading to an increase in crosstalk.

The magnitude of crosstalk due to this effect is modelled by applying the filter response to each of the most significant harmonics individually. The most significant should be those closest to the measurement band. The amplitude of the three most relevant harmonics (annotated in Fig. 11) after being filtered by a Mth order CIC filter for crosstalk originating from a normalized $s_{het} \downarrow$ crosstalk signal with optical phase frequency, f_{sig}, are given in Eqn. 21.

$$h_0 = \frac{1}{L}\left(\frac{f_s}{\pi f_{sig}}\sqrt{\sin^2\left(\frac{\pi L f_{sig}}{f_{chip}}\right)}\right)^M \tag{21a}$$

$$h_{1a} = \frac{2^{k/2}}{L}\left(\frac{f_s}{\pi(f_{code}-f_{sig})}\sqrt{\sin^2\left(\frac{\pi L(f_{code}-f_{sig})}{f_{chip}}\right)}\right)^M \tag{21b}$$

$$h_{1b} = \frac{2^{k/2}}{L}\left(\frac{f_s}{\pi(f_{code}+f_{sig})}\sqrt{\sin^2\left(\frac{\pi L(f_{code}+f_{sig})}{f_{chip}}\right)}\right)^M \tag{21c}$$

Optics EXPRESS

The values $\frac{1}{L}$ and $\frac{2^{k/2}}{L}$ correspond to the input amplitudes of the PRBS harmonics for the $s_{het}\downarrow$ crosstalk signal. For the signals originating from the s_{hom} and $s_{het}\uparrow$ components, the harmonic in the measurement band is dependent on the heterodyne frequency. The compatibility with previous descriptions can be seen when considering a slow moving phase signal, i.e. when $f_{sig} = 0$, the only remaining amplitude is from the harmonic in the measurement band, $\frac{1}{L}$ which corresponds to the correlation of M-sequences. This description however predicts a decrease in suppression of incorrectly decoded signals as f_{sig} increases towards f_{code}. Increasing the filter order has the advantage of decreasing the influence of the higher frequency harmonics, but will also slightly reduce the effective measurement bandwidth. The second order CIC was chosen to balance measurement bandwidth and attenuation of higher frequency harmonics. Another consideration is the practical hardware consumption required for implementation of higher order filters. Similar tradeoffs in choice of CIC filter order have been discussed in reference to the deep phase modulation interferometry technique [29].

Eqn. 21 displays the filtered magnitude of each harmonic, however, they are all present simultaneously and potentially alias to the same frequency in the measurement band after rate reduction. The addition of harmonics which alias to the same frequency will depend on their relative phase, with the origin of PRBS harmonic phases being the delay relative to the start of the filtering sum and the specific PRBS sequence. This results in a code delay dependence for crosstalk originating from signals with more than one significant PRBS harmonic, such as high frequency signals. In a physical implementation it may not be possible to explicitly control the relative delay of the signals. An average value for the amplitude of suppressed signals is obtained by adding the amplitude of the PRBS harmonics in quadrature, as shown in Eqn. 22.

$$\eta(f_{sig}) = \sqrt{h_0(f_{sig})^2 + h_{1a}(f_{sig})^2 + h_{1b}(f_{sig})^2} \tag{22}$$

The crosstalk described here is directly applicable for relatively narrow phase signals in the measurement band. For wider signals, the crosstalk should increase as more harmonics contribute. This culminates in a white noise signal, which is not suppressed at all.

3.3.3. Magnitude of crosstalk between two channels

To quantitatively measure crosstalk from a single suppressed channel, the suppressed tone ratio as described in Eqn. 18 was recorded for a range of tone frequencies (varying ω_ξ) within the measurement band. This test used the heterodyne frequency $f_{het} = f_{chip} - f_{code}$, and a 2nd order CIC filter. A version is also included for 7, 8 and 9 bit codes (three different code lengths) to verify the ability reduce crosstalk by increasing the codelength. For higher frequency phase signals, the amount of suppression is expected to be dependent on the delay of the incorrectly decoded sequence. In order to get a "typical" value for crosstalk, phase data was recorded at each possible delay of the suppressed channel, with 12000 points per delay. The reported suppression value for each frequency is the average of the crosstalk measured at each delay (excluding the delay of channel 1).

The experimental measurements are compared with the analytically expected crosstalk in Fig. 12. The analytically expected crosstalk was given previously in Eqn. 18 and uses $\eta(f_{sig})$ from Eqn. 22. The analytical expression was adjusted for the unequal power between signal channels measured at: $\frac{A_2}{A_1} \approxeq 0.86$. The points denote the experimental data, with error bars calculated based on 3 repetitions of these data sets. The dashed lines are the analytically predicted crosstalk values.

The crosstalk predicted analytically and observed in the experiment follow similar trends, a flat region at low frequencies followed by an increase in crosstalk with the frequency of the injected tone. This increase in crosstalk was expected as higher frequency harmonics outside of the measurement bandwidth are less attenuated. The experimental crosstalk at low frequencies,

Optics EXPRESS

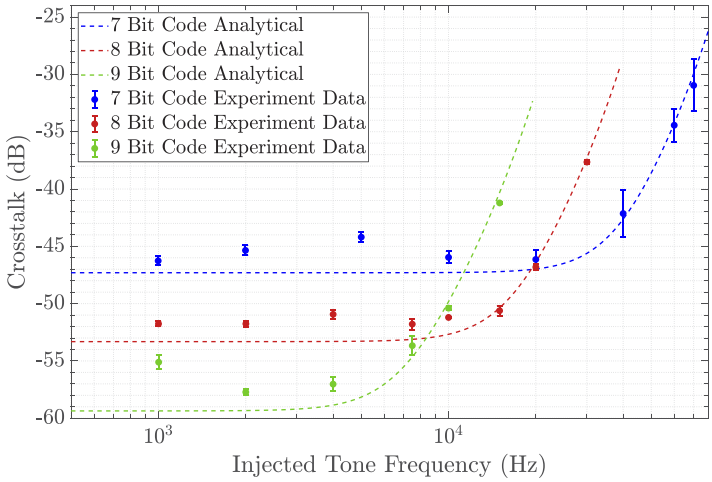

Fig. 12. Dependence of crosstalk suppression on signal frequency (f_{sig}) for different codelengths. Compared are the analytically expected crosstalk (dashed) and the mean experimentally measured crosstalk (dots).

was slightly increased in comparison to the value predicted analytically. The magnitude of the error bars in comparison to the deviation from the analytically predicted crosstalk indicates that there are factors such as subchip delay mismatches and bandwidths effects degrading suppression of crosstalk rather than variability due to changing phase noise from test to test.

Increasing the codelength was able to reduce the low frequency crosstalk level. A potential limit on reducing crosstalk by increasing codelength is the point at which the contribution resulting from the spikes induced by bandwidth limits begin to dominate. Additionally, each increased step in codelength corresponds to an approximately 50% reduction in the measurement bandwidth.

3.4. Scaling of crosstalk with number of channels

To measure the scaling of crosstalk with number of channels, up to five channels were sequentially added to the signal arm, each phase modulated with an M-sequence PRBS, and channels 2-5 driven with a 2 kHz phase modulation. The heterodyne frequency for this test was set to $f_{het} = f_{chip} - f_{code}$ and a 2nd order CIC filter was used. The delay of the PRBS applied to each additional channel was separated by at least a whole chip, then optimised by testing adjacent subchip delays and using the delay which generated the least crosstalk. It should be noted that the arrangement of EOMs resulted in double the power in channel 1 compared to the other channels, which is expected to decrease the crosstalk by 3 dB.

Unlike the randomly fluctuating optical phase, the phase of the tone injected on suppressed channels was directly controlled on the FPGA. To represent a typical interferometry system, uncorrelated phase noise at the tone frequency was imitated by randomizing the phase of the injected tone between $-\pi$ and π on channels 2-5. Phase data was recorded for ten sets of randomized phase. A measurement of crosstalk from each set of channels individually was also recorded, i.e. where the optical signals present were Ch1+Ch2, Ch1+Ch3, Ch1+Ch4 and Ch1+Ch5. When multiple channels are present simultaneously, the crosstalk is measured as the ratio of the amplitude of the 2 kHz tone in channel 1 to the mean injected tone amplitude in the

Optics EXPRESS

other channels according to:

$$\text{Crosstalk}(N) = 20\log_{10}\left(\frac{\bar{\xi}_1}{\left(\sum_{n=1;n\neq 1}^{N}\bar{\xi}_n\right)/(N-1)}\right)[dB] \tag{23}$$

Where $\bar{\xi}_n$ is measured amplitude of the injected tone in channel n.

Measurements of the 2 kHz tone's amplitude in channel 1 due to crosstalk as the number of channels in the signal arm was increased are shown in Fig. 13(a). The mean crosstalk when the tone phase was randomized is greater than the direct sum of the crosstalk measured from each channel individually for a 20 MHz chip frequency. This is attributed to increasing influence of homodyne interference which is expected to scale linearly in comparison to the square-root scaling expected from crosstalk from heterodyne interference.

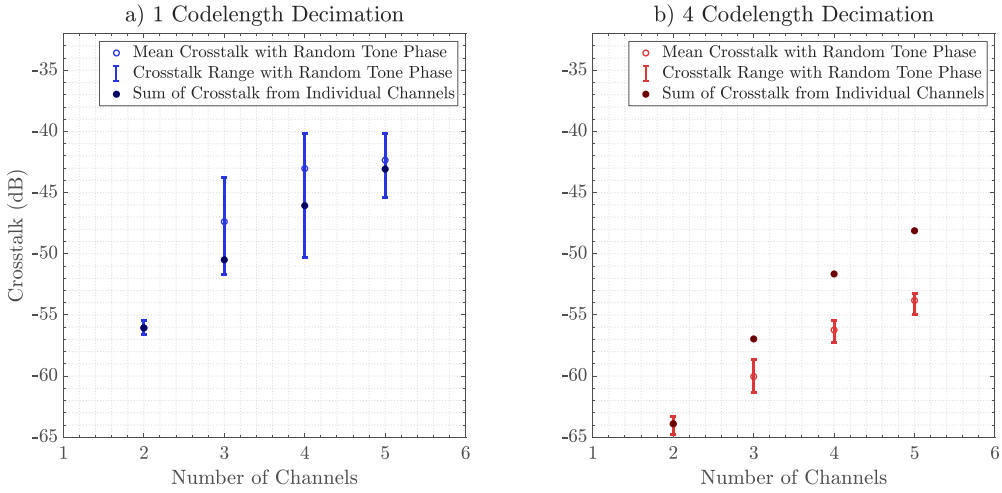

Fig. 13. Scaling of crosstalk with an increasing number of channels. The dot represents the mean crosstalk across all randomized tone phases. The bars represent the measured range of crosstalk as the phase difference between the injected tones is changed. a) Shows the increase in crosstalk with number of channels when setting the low pass filter decimation equal to the code length and heterodyne frequency to $f_{het} = f_{chip} - f_{code}$. b) Shows a reduced increase in crosstalk when averaging over four codelengths and setting the heterodyne frequency to $f_{het} = f_{chip} - 1.25 f_{code}$.

We now propose an alternative configuration to remove crosstalk from the s_{hom} and $s_{het}\uparrow$ based on the ability to shift the crosstalk described in Eqn. 20. When the filter decimation is set to a single codelength and the heterodyne frequency is changed, as one PRBS harmonic moves out the measurement band, another harmonic moves in. Setting the decimation to four codelengths and shifting the heterodyne frequency by a quarter of the code frequency will cause all harmonics from s_{hom} and $s_{het}\uparrow$ to be shifted into a low pass filter null. That is, $R = 4L\frac{f_s}{f_{chip}}$ and $f_{het} = (K - 0.25)f_{code}$ (where K is an integer). The tradeoff for this configuration is a four times reduction in the measurement band and there will still be crosstalk originating from the $s_{het}\downarrow$ signals.

With this configuration applied, the crosstalk measurement when scaling the number of channels was repeated and is shown in Fig. 13(b). The increase in crosstalk with number of channels is now less than the direct sum and there is also an overall reduction in the level of crosstalk. This is consistent with the previous configuration being influenced by s_{hom} and $s_{het}\uparrow$, now more strongly attenuated.

Optics EXPRESS

The suitability of a given configuration will depend on the requirements of a given application. The configuration which sets the decimation to four times the code length and offsets the heterodyne frequency by a quarter of the code frequency is ideal for applications which benefits from minimal crosstalk and require a large number of channels. However, for applications which benefit from a wide measurement band, it may be unnecessary. Additionally, minimizing subchip delays through control of the PRBS travel time for each channel and use of RF equipment that minimally degrades the PRBS may decrease the crosstalk from s_{hom} sufficiently in configurations with decimation set to single codelength.

4. Predicted performance for many channels

Based on the expected and observed crosstalk of a DEHI phase measurement system in the previous sections and known behaviour of heterodyne interferometry, the potential number of simultaneously supported channels, N, is discussed. The properties of a DEHI system which relate to potential limitations to the number of channels are summarized in Table 3.

Table 3. Scaling of key DEHI parameters with number of channels, N and optical powers P_{LO} and P_n. A change in notation is used for brevity, where $\Lambda_{het\downarrow}$, $\Lambda_{het\uparrow}$ and $\Lambda_{hom\downarrow}$ represent the crosstalk fraction from a single suppressed signal

Property	Analytically Predicted Value
Required unique delays	a) $N \leq L$ b) $N + \frac{N^2-N}{2} \leq L$
DC photodetector power	$P_{LO} + NP_n$
AC coupled signal power (average)	$\sqrt{NP_{LO}P_n + \frac{N^2-N}{2}P_n^2}$
Crosstalk (downshifted heterodyne terms)	$\sqrt{\Lambda_{het\downarrow}^2(N-1)}$
Crosstalk (all terms)	$\sqrt{\Lambda_{het\downarrow}^2(N-1) + \Lambda_{hom}^2\frac{N^2-N}{2}\frac{P_n}{P_{LO}} + \Lambda_{het\uparrow}^2(N-1)}$
Detector noise	$\frac{\sigma_{dark}}{\sqrt{P_{LO}P_n}}$
Phase shot noise	$\sqrt{\frac{\hbar c}{2\pi}\frac{(P_{LO}+NP_n)}{\lambda P_{LO}P_n}}$

At a basic level, there needs to a be a unique delay (or code) for each channel to be measured unambiguously, described in row 1 of Table 3. If only the heterodyne interference terms are significant, case a), it is sufficient to have the number of channels less than the code length. However homodyne interference terms appear at a generally unknown delay in the sequence as per Eqn. 5. These are included in case b), where a unique delay would also be need for each of the homodyne interference signals, requiring a longer codelength if the chosen low pass filter is unable to sufficiently remove the decoded and demodulated homodyne signal.

The second and third row concern limits on the detector. The DC photodetector power is the sum of the individual local oscillator and signal arm powers and increases linearly with the number of channels. It governs whether the system reaches the damage threshold of the detector (typically thermally limited). With full modulation depth on the PRBS, the majority of the frequency content of the s_{hom} signals will be "fast" and not contribute to this power. For partial modulation depths there will be some contribution not removed by AC coupling depending on the relation between the phase noise and the low frequency cut-off.

The AC coupled photodetector power will govern whether the detection system saturates, relevant to photodetector and ADC. The AC coupled power was estimated by adding the power of each signal from s_{het} and s_{hom} in quadrature. This results in square-root scaling of the AC coupled power from the heterodyne interference signals and linear scaling from homodyne interference signals with number of channels. The validity of this description is dependent on the phase difference between each signal being random, the signals having full modulation depth and interference visibility. In a real system, non-linearity and slew-rate limits when operating near the limits of the detection system may also limit power and degrade high frequency signals.

Optics EXPRESS

For both forms of power, a linear decrease in signal arm power with number of channels would limit their growth to prevent detector damage or saturation. By design, fiber based combination of signals to a single photodetector will on average involve a linear reduction in the signal arm power when comparing before the 50/50 beam-splitters to after the splitters. It should be noted that practically, additional losses due to the increased fiber lengths and splitter imperfections would further decrease the optical power.

Two cases for the scaling of crosstalk are considered. The first, preferable case, has the crosstalk limited to the $s_{het} \downarrow$ components. This would result in scaling of crosstalk proportional to the square-root of the number of channels and may be experimentally achieved by setting the filter decimation to four times the code length (with discussed heterodyne frequency) or by avoiding the bandwidth limitations on the PRBS generation and modulation. In the second case, the crosstalk originating from s_{hom} is not negligible. With no other change, this case is expected to cause scaling of crosstalk to be linear with the number of channels. To limit scaling of crosstalk when s_{hom} signals are not negligible, a linear reduction in signal arm power with number of channels could be applied, matching the scaling of the s_{hom} terms to the s_{het} terms. A quadratic decrease in signal arm power would be required to prevent any increases in the contribution from the s_{hom} terms. An increase in local oscillator power would also decrease the relative influence of s_{hom}, however, this is limited by saturation of the detection system.

The number of channels where the expected crosstalk reaches 1% of a targeted channel's phase (or −20 dB in power) of the correctly decoded signal is plotted for two different ratios of local oscillator to signal arm power as a function of code length in Fig. 14(a). A version is also shown where crosstalk solely originates from $s_{het} \downarrow$ signals. This case results in the greatest number of supported channels, approaching 1000 channels with a 2047 chip length code. Implementing a linear reduction in signal arm power also appears to allow for hundreds of channels while having crosstalk from s_{hom} signals and no reduction in signal arm power significantly reduces the number of supported channels. It should also be noted that if the cause of the homodyne terms being present in the phase readout are the spikes originating from bandwidth effects, increasing the codelength won't improve the suppression. However, decreasing the signal arm power as the number of channels increases should still reduce their impact. While this provides an estimate of the scaling of the number of channels supported, the specific number will depend on the ability to make $\Lambda = \frac{1}{L}$ and the acceptable crosstalk level.

Whether to prevent saturation or to reduce crosstalk, a consequence of reducing the signal arm power levels is an increase in the prevalence of dark-noise from the photodetector or ADC as well as shot noise. The expression for detector noise is generalized by parameter σ_{dark} in Table 3, which will be dependent on the particular equipment used, however, the proportionality to the local oscillator and signal arm power will remain. The shot noise is dependent only on the ratio of total optical power to the power of the targeted signal, rather than the components used.

The detector noise and phase shot noise level was calculated for a linear reduction in signal arm power and is shown in Fig. 14(b). The local oscillator power used was 10 μW, near the level where saturation behaviour was observed in the experiment. The value for σ_{dark} was set so that the phase noise with a single channel was equal to 1 $\mu\text{Cycle}/\sqrt{\text{Hz}}$.

For the chosen parameters, detector dark noise contributes noise at least an order of magnitude greater than shot noise. The dark noise level will depend on the characteristics of the photodetector and ADC, while reducing the shot noise requires being able to measure higher powers. Scalar adjustments to the curves can be used to make this description compatible with the capabilities of particular detection systems, corresponding to changes in local oscillator or signal arm power.

Optics EXPRESS

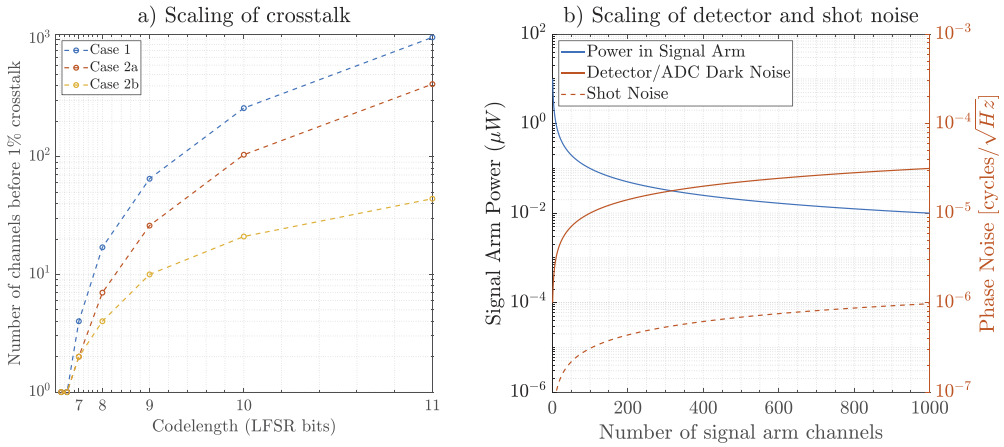

Fig. 14. a) Predicted number supported channels before reaching 1% crosstalk depending on ability to suppress crosstalk for different local oscillator, signal arm power ratios. Case 1 is crosstalk solely from $s_{het} \downarrow$ signals, case 2a is crosstalk from all signals with $1/N$ signal arm power scaling and case 2b is the crosstalk from all signals with no power scaling. b) Simulated detector noise and shot noise when changing the signal arm power to accommodate an increased number of channels according to $P_n = \frac{P_L O}{N}$.

5. Conclusion

In this work, we established a comprehensive accounting of the potential crosstalk when measuring the phase of multiple optical fields simultaneously using Digitally Enhanced Heterodyne Interferometry.

Parameters were established to reduce crosstalk and an experimental demonstration showed suppression of phase crosstalk from a single channel close to the limit set by the M-sequence PRBS used of $\approxeq$ 55 dB with a 20 kHz measurement bandwidth. This required setting the low pass filter decimation equal to the codelength and setting the heterodyne frequency to $f_{het} = f_{chip} - f_{code}$. This heterodyne frequency was required to mitigate the practical effects which were found to potentially limit suppression of crosstalk. These were bandwidth limitations on the modulation of PRBS and misaligned chip transitions.

The experimental demonstration also showed the importance of limiting the influence of crosstalk originating from the homodyne interference between signal arms. Successfully suppressing these terms is the difference between a linear or square-root scaling of crosstalk with number of channels. A new configuration more suitable for suppressing crosstalk from a large number of channels by suppressing homodyne interference was established. This set $f_{het} = f_{chip} - 0.25 f_{code}$ and low pass filter decimation to four times the codelength.

The expected potential limitations when scaling to a large number of simultaneous phase measurements were outlined. A linear reduction in the power of the signal arm is proposed to prevent saturation of the detection system and assist with the reduction of homodyne interference contributing to crosstalk. The associated increases in detector dark noise and shot noise were outlined. 100's to 1000's of channels are expected to be supported depending on the capabilities of the components used and requirements on measurement noise.

Funding

Australian Research Council Centre of Excellence for Gravitational Wave Discovery (CE170100004; Australian Research Council Centre of Excellence for Engineered Quantum Systems CE170100009).

Optics EXPRESS

Acknowledgments

P. Sibley and R. Ward would like to acknowledge support from the Breakthrough Initiatives. P. Sibley would also like to acknowledge the support of the Cooperative Research Centre for Space Environment Management (SERC Limited) through the Australian Government's Cooperative Research Centre Programme and is supported by an Australian Government Research Training Program (RTP Scholarship).

Disclosures

The authors declare no conflict of interests.

References

1. D. A. Shaddock, "Digitally enhanced heterodyne interferometry," Opt. Lett. **32**(22), 3355–3357 (2007).
2. R. Scholtz, "The origins of spread-spectrum communications," IEEE Trans. Commun. **30**(5), 822–854 (1982).
3. K. Fouli and M. Maier, "Ocdma and optical coding: Principles, applications, and challenges [topics in optical communications]," IEEE Commun. Mag. **45**(8), 27–34 (2007).
4. B. Pulford, "Locset phase locking: operation, diagnoistics, and applications," Thesis (2012).
5. C. A. Lu, A. Flores, E. Bochove, W. P. Roach, V. Smirnov, and L. B. Glebov, "Active coherent superposition of five fiber amplifiers at 670w using multiplexed volume bragg gratings," pp. 86011A–86011A–6.
6. A. Klenke, M. Müller, H. Stark, A. Tünnermann, and J. Limpert, "Sequential phase locking scheme for a filled aperture intensity coherent combination of beam arrays," Opt. Express **26**(9), 12072–12080 (2018).
7. H. K. Ahn and H. J. Kong, "Cascaded multi-dithering theory for coherent beam combining of multiplexed beam elements," Opt. Express **23**(9), 12407–12413 (2015).
8. T. M. Shay, "Theory of electronically phased coherent beam combination without a reference beam," Opt. Express **14**(25), 12188–12195 (2006).
9. Y. Ma, X. Wang, J. Leng, H. Xiao, X. Dong, J. Zhu, W. Du, P. Zhou, X. Xu, L. Si, Z. Liu, and Y. Zhao, "Coherent beam combination of 1.08 kw fiber amplifier array using single frequency dithering technique," Opt. Lett. **36**(6), 951–953 (2011).
10. Y. Ma, P. Zhou, X. Wang, H. Ma, X. Xu, L. Si, Z. Liu, and Y. Zhao, "Active phase locking of fiber amplifiers using sine–cosine single-frequency dithering technique," Appl. Opt. **50**(19), 3330–3336 (2011).
11. A. Azarian, P. Bourdon, L. Lombard, Y. Jaouën, and O. Vasseur, "Orthogonal coding methods for increasing the number of multiplexed channels in coherent beam combining," Appl. Opt. **53**(8), 1493–1502 (2014).
12. M. Jiang, R. Su, Z. Zhang, Y. Ma, X. Wang, and P. Zhou, "Coherent beam combining of fiber lasers using a cdma-based single-frequency dithering technique," Appl. Opt. **56**(15), 4255–4260 (2017).
13. T. Kissinger, T. O. H. Charrett, and R. P. Tatam, "Range-resolved interferometric signal processing using sinusoidal optical frequency modulation," Opt. Express **23**(7), 9415–9431 (2015).
14. A. Goldsmith, ed., *Spread Spectrum* (Cambridge University Press, Cambridge, 2005), pp. 403–451.
15. S. P. Francis, T. T. Y. Lam, D. E. McClelland, and D. A. Shaddock, "Multi-link laser interferometry architecture for interspacecraft displacement metrology," J. Geod. **92**(3), 241–251 (2018).
16. Y. Zhang, C. P. Bandutunga, M. B. Gray, and J. H. Chow, "Multi-target cw interferometric acoustic measurements on a single optical beam," Opt. Express **27**(13), 18477–18483 (2019).
17. S. Ngo, T. G. McRae, M. B. Gray, and D. A. Shaddock, "Homodyne digital interferometry for a sensitive fiber frequency reference," Opt. Express **22**(15), 18168–18176 (2014).
18. N. Riesen, T. T. Y. Lam, and J. H. Chow, "Bandwidth-division in digitally enhanced optical frequency domain reflectometry," Opt. Express **21**(4), 4017–4026 (2013).
19. D. Tarquin Ralph, P. A. Altin, D. S. Rabeling, D. E. McClelland, and D. A. Shaddock, "Interferometric wavefront sensing with a single diode using spatial light modulation," Appl. Opt. **56**(8), 2353–2358 (2017).
20. L. E. Roberts, R. L. Ward, A. J. Sutton, R. Fleddermann, G. de Vine, E. A. Malikides, D. M. R. Wuchenich, D. E. McClelland, and D. A. Shaddock, "Coherent beam combining using a 2d internally sensed optical phased array," Appl. Opt. **53**(22), 4881–4885 (2014).
21. L. E. Roberts, R. L. Ward, S. P. Francis, P. G. Sibley, R. Fleddermann, A. J. Sutton, C. Smith, D. E. McClelland, and D. A. Shaddock, "High power compatible internally sensed optical phased array," Opt. Express **24**(12), 13467–13479 (2016).
22. S. Ngo, D. A. Shaddock, T. G. McRae, T. T. Y. Lam, J. H. Chow, and M. B. Gray, "Suppressing rayleigh backscatter and code noise from all-fiber digital interferometers," Opt. Lett. **41**(1), 84–87 (2016).
23. D. M. R. Wuchenich, T. T. Y. Lam, J. H. Chow, D. E. McClelland, and D. A. Shaddock, "Laser frequency noise immunity in multiplexed displacement sensing," Opt. Lett. **36**(5), 672–674 (2011).
24. R. N. Mutagi, "Pseudo noise sequences for engineers," Electron. Commun. Eng. J. **8**(2), 79–87 (1996).
25. D. Shaddock, B. Ware, P. G. Halverson, R. E. Spero, and B. Klipstein, "Overview of the lisa phasemeter," AIP Conf. Proc. **873**, 654–660 (2006).
26. L. E. Roberts, "Internally sensed optical phased arrays," Thesis (2016).

Optics EXPRESS

27. B. Canuel, E. Genin, G. Vajente, and J. Marque, "Displacement noise from back scattering and specular reflection of input optics in advanced gravitational wave detectors," Opt. Express **21**(9), 10546–10562 (2013).
28. K.-S. Isleif, O. Gerberding, S. Köhlenbeck, A. Sutton, B. Sheard, S. Goßler, D. Shaddock, G. Heinzel, and K. Danzmann, "Highspeed multiplexed heterodyne interferometry," Opt. Express **22**(20), 24689–24696 (2014).
29. T. S. Schwarze, O. Gerberding, F. G. Cervantes, G. Heinzel, and K. Danzmann, "Advanced phasemeter for deep phase modulation interferometry," Opt. Express **22**(15), 18214–18223 (2014).